

# Resource-efficient digital bosonic quantum simulations

Marco Majland<sup>1</sup> and Nikolaj Thomas Zinner<sup>1,2</sup>

<sup>1</sup>*Department of Physics and Astronomy, Aarhus University, Ny Munkegade 120, 8000 Aarhus C, Denmark*<sup>\*</sup>

<sup>2</sup>*Aarhus Institute of Advanced Studies, Aarhus University,  
Høegh-Guldbergs Gade 6B, 8000 Aarhus C, Denmark*

(Dated: March 1, 2025)

Quantum algorithms are promising candidates for the enhancement of computational efficiency for a variety of computational tasks, allowing for the numerical study of physical systems intractable to classical computers. In the Noisy Intermediate Scale Quantum (NISQ) era of quantum computing, however, quantum resources are limited and thus quantum algorithms utilizing such resources efficiently are highly coveted. We present a resource-efficient quantum algorithm for bosonic quantum simulations using the Variational Quantum Eigensolver algorithm with the Unitary Coupled Cluster ansatz. Our algorithm proves to significantly increase accuracy with a simultaneous large reduction of required quantum resources, exhibiting increased performance for all relevant parameters compared to current approaches. It provides a shorter route to achieve a quantum advantage in bosonic quantum simulations along with a flexible method to tailor the utilized quantum resources of a quantum computer. While being specifically feasible for NISQ devices, the advantages of our algorithm are independent of hardware parameters, maintaining its superiority for future fault-tolerant quantum devices. The study of vibrational properties of molecular systems is crucial in a variety of contexts, such as spectroscopy, fluorescence, chemical reaction dynamics and transport properties. Thus, our algorithm provides a resource-efficient flexible approach to study such applications in the context of quantum computational chemistry on quantum computers.

## I. INTRODUCTION

The digital simulation of many-body physics is one of the most promising applications of quantum computers [1]. Yet, current Noisy Intermediate Scale Quantum (NISQ) devices are faced with the challenges of limited quantum resources such as qubit memory and quantum gate fidelities [2]. For quantum algorithms to be feasible for such devices, it is crucial to consider algorithms which reduce the required resources for equivalent computations [3–9]. With bosonic quantum simulations possibly providing a platform to achieve an early quantum advantage for practical tasks compared to its electronic counterpart, the development of resource-efficient bosonic quantum algorithms is crucial [10]. A highly pursued application of quantum computing is quantum computational chemistry [11], for which significant developments have been made in the numerical study of molecular systems using the Variational Quantum Eigensolver (VQE) algorithm [12–16]. Specifically, the study of the vibrational properties of molecular systems is crucial in a variety of contexts, such as spectroscopy, fluorescence, chemical reaction dynamics and transport properties [14, 17–20]. A general framework to compute bosonic spectra using the VQE with the Unitary Coupled Cluster (UCC) ansatz has been developed based on a direct mapping (DM) protocol [15]. However, the current approaches suffer from inaccuracy and require a substantial amount of quantum resources, being infeasible specifically in the near-term NISQ era perspective.

In our work, we present a resource-efficient non-heuristic algorithm, the Compact Encoding Algorithm (CEA), for bosonic quantum simulations. The algorithm combines two

strategies which give rise to an increased accuracy, a polynomial increase of qubit memory and a simultaneous significant reduction of the required quantum resources, exhibiting increased performance for all relevant parameters. Since smaller qubit registers and shallower circuit depths give rise to much lower probabilities of errors, such reductions yield substantially increased accuracy while utilizing fewer quantum resources.

## II. THEORETICAL BACKGROUND

Compared to the two-body Coulomb interactions of electronic systems, an interacting system of bosons exhibits many-mode couplings which further complicates the structure of the Hamiltonian. One way to parametrize a many-body system of interacting bosons is to expand the interaction term in a so-called  $n$ -body expansion [21, 22]. In this expansion, each bosonic mode is expanded into a spectrum of modals for which the total state of the system is described as a product state of occupation number vectors designating the modal occupations for each mode, called a Hartree product. This formalism and the UCC ansatz are used in the following sections for which additional details may be found in Appendix A and C, respectively.

## III. COMPACT ENCODING ALGORITHM

In the following, we describe two strategies to efficiently utilize the available quantum resources and thus increase the precision of bosonic quantum simulations. Analytical estimations of the reduction of 2-qubit gates are presented in Appendix D.

\* [majland@phys.au.dk](mailto:majland@phys.au.dk)

### A. Strategy 1: Hamming truncation

Different encoding approaches for  $d$ -level quantum simulations have been investigated [6], although compact approaches in quantum computational chemistry have generally been discarded due to the increase of required quantum gate resources [15]. In general, a compact encoding increases the relative Hamming distance between the encoded qubit states, increasing the complexities of the cluster operators, leading to larger circuit depths.

#### Hamming distance

For two binary strings, the Hamming distance is defined as the amount of bits differing between the two strings. As an example, consider the strings 001 and 101. For these two strings,  $dh(001, 101) = 1$  since the first bit entry differs.

In the DM, a modal occupation is mapped to the state of a qubit, utilizing only a minor subspace of the qubit Hilbert space, for which the modal space dimensionality equals the available number of qubits. To obtain the same modal space dimensionality with a logarithmic reduction of qubit resources, the modal occupations may be encoded using binary decomposition [23].

Consider a bosonic system with  $L$  modes with modal dimension  $N_l$  for mode  $l$ . A configuration for such a system may be parametrized by a configuration vector,  $\mathbf{r} = [r^0, \dots, r^{L-1}]^T$ , with  $\{r^l\}$  designating the indices of the occupied modals. The corresponding Hartree product reads

$$\begin{aligned} |\Phi_{\mathbf{r}}\rangle &= |r^0\rangle \otimes \dots \otimes |r^{L-1}\rangle \quad (1) \\ &= \underbrace{\left( \bigotimes_{i=0}^{\log_2(N_0)-1} |r_i^0\rangle \right)}_{\text{Mode 0 register}} \otimes \dots \otimes \underbrace{\left( \bigotimes_{i=0}^{\log_2(N_{L-1})-1} |r_i^{L-1}\rangle \right)}_{\text{Mode L-1 register}} \quad (2) \end{aligned}$$

where  $r_i^l \in \{0, 1\}$  is the  $i$ 'th coefficient in the binary decomposition of  $r^l$ .

The mapping of the annihilation operator is defined as

$$a_{r^l}^l \rightarrow \bigotimes_{i=0}^{\log_2(N_l)-1} \left( \sigma_i^{l+} \right)^{r_i^l} \quad (3)$$

where the Pauli operator acts on the  $i$ 'th qubit in the  $l$ 'th register. The analogous definition holds for the Hermitian conjugate of Eq. 3.

When implemented on a quantum computer, the UCC ansatz is decomposed in a Trotter expansion which allows for the sequential operation of quantum logic gates on the reference Hartree product. Using Eq. 3, excitation operators for the UCC transform as

$$a_{r^l}^{l\dagger} a_{s^l}^l \rightarrow \bigotimes_{i=0}^{\log_2(N_l)-1} \left( \sigma_i^{l+} \right)^{r_i^l} \left( \sigma_i^{l-} \right)^{s_i^l}. \quad (4)$$

All encoded qubit states in the DM differ by only one qubit, yielding a Hamming distance of  $dh = 1$  for all states. With reference to Eq. 4, a cluster excitation operator in the DM exhibits the same Pauli structure for all excitations. This is generally not true for the CEA, since the CEA contains states with  $dh > 1$ . For  $dh = 2$ , according to Eq. 4, this yields a product of four Pauli raising/lowering operators. Subtracting the Hermitian conjugate yields a total of 8 terms of Pauli operators with 4 products in each term. To avoid lengthy Pauli terms while maintaining an advantage over the DM, one may truncate the Hilbert space to contain only qubit states with a Hamming distance below a given threshold. Thus, one may decompose the qubit Hilbert space into two subspaces,

$$\mathcal{H} = \mathcal{H}_{\text{enc}} \cap \mathcal{H}_{\text{trun}} \quad (5)$$

where  $\mathcal{H}_{\text{enc}}$  is the subspace of qubit states available for encoding and  $\mathcal{H}_{\text{trun}}$  is the truncated subspace. The result of the Hamming truncation produces  $\mathcal{H}_{\text{enc}}$  which requires a shallower circuit depth for implementation. With  $dh_{\text{max}}$  denoting the Hamming threshold and  $N$  the qubit register size, the dimensional scalings of  $\mathcal{H}_{\text{enc}}$  are  $\dim(\mathcal{H}_{\text{enc}}^{\text{DM}}) \sim \mathcal{O}(N)$  and  $\dim(\mathcal{H}_{\text{enc}}^{\text{CEA}}) \sim \mathcal{O}(N^{dh_{\text{max}}})$ , as is elaborated in Appendix B. Thus, for a given set of available qubit resources, the CEA exhibits a polynomial qubit memory advantage as compared to the DM. The binary decomposition of the modal indices, however, no longer necessarily correspond to the qubit states. One may therefore transform the modal states into, in principle, arbitrary qubit states.

While the Hamming truncation provides a method to increase accuracy and reduce the gap to quantum advantage for near-term devices, the method also provides encoding flexibility for future fault-tolerant quantum devices by appropriately choosing the Hamming threshold based on the preferences of the hardware parameters.

### B. Strategy 2: Ground state encoding protocol

To further reduce the circuit depth of the implementation of the UCC on a quantum computer, one may choose to encode the reference modal states into the qubit ground states. This is achieved by re-organizing the modal basis elements for each mode such that the modals contained in the reference configuration obtain the label  $s^l = 0$ . With this re-ordering, all reference modals are transformed into their respective qubit register ground states,  $|0\dots0\rangle$ . This has no physical implications since the ordering of basis elements is arbitrary. The excitation operators then reduce significantly with

$$\bigotimes_{i=0}^{\log_2(N_l)-1} \left( \sigma_i^{l+} \right)^{r_i^l} \left( \sigma_i^{l-} \right)^{s_i^l} = \bigotimes_{i=0}^{\log_2(N_l)-1} \left( \sigma_i^{l+} \right)^{r_i^l}. \quad (6)$$

This is the case since  $s_i^l = 0$  for all  $i$  and all  $l$  in the reference Hartree product. Thus, all annihilation operators equal the identity operator, yielding significantly less terms in the exponential of the UCC ansatz and thus a more shallow circuit depth.

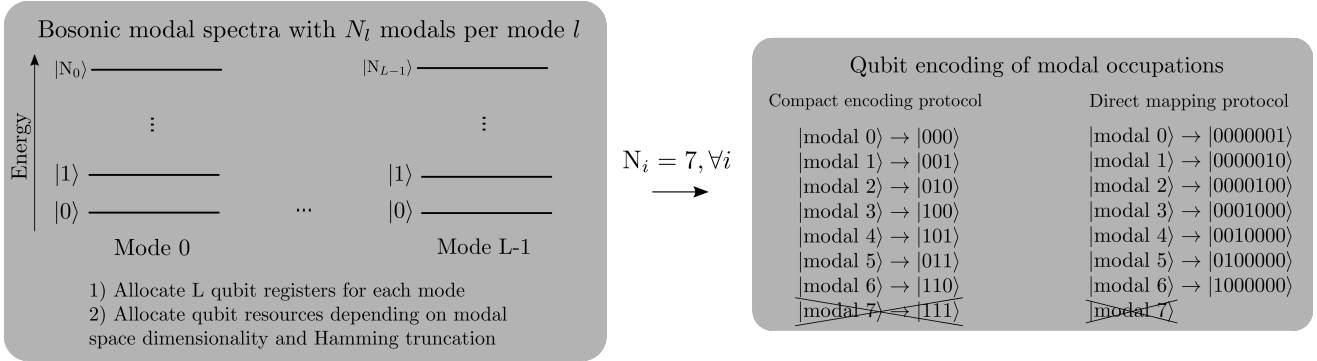


FIG. 1. Illustration of the two strategies of the CEA. For each mode spectrum, one may choose a modal space dimensionality which appropriately utilizes the qubit resources. With a Hamming truncation  $dh_{\max} = 3$ , one may encode 2 modal states into 1 qubit, 4 modal states into 2 qubits, 7 modal states into 3 qubits, etc. Thus, one may achieve a polynomial increase in the qubit register memory with the CEA as compared to the DM.

### C. Summary of the CEA

The two strategies of the CEA are summarized in the following.

1. Choose appropriate modal space dimensions for each mode based on the qubit register sizes and Hamming truncation to maximize the utilized qubit states in  $\mathcal{H}_{\text{enc}}$ .
2. Encode the modal states into the qubit states with the modal ground state encoded into the qubit ground state.

An illustrative figure of the encoding protocol is depicted in Fig. 1.

To summarize, the first strategy (Hamming truncation) provides a flexible method to provide a large (small) qubit memory advantage with a small (large) circuit depth reduction. Independent of the degree of truncation, the CEA provides a polynomially higher qubit memory compared to the DM with the circuit depth reduction scaling with the Hamming truncation. The second strategy (ground state encoding protocol) involves the encoding of ground state modals into the qubit ground states, utilizing the structure of the  $n$ -body formalism excitation spectra. These two strategies of the CEA allows for resource-efficient quantum computations not only for short-term but also long-term quantum devices.

## IV. NUMERICAL RESULTS

In the following, we present a comparative study of the computational performances of the CEA and the DM using the common benchmark molecule,  $\text{CO}_2$ . For  $\text{CO}_2$ , we calculate the ground state energy along with three excited state energies using the Quantum Equation of Motion (QEOM) algorithm [24] and compare the results to reference energies (exact diagonalization of the Hamiltonian). This allows for a comparative study of precision and a demonstration of a large reduction of the gap to quantum advantage for bosonic quantum simulations.

All VQE computations are simulated with the noisy device

QASM simulator using an extended version of the IBM Qiskit software package [25] implementing the CEA. All four vibrational modes of  $\text{CO}_2$  are included with two modal wavefunctions per mode, requiring four qubits for the CEA and eight qubits for the DM. We sample ground and excited state energies with 300 samples for both the CEA and the DM. Further computational details are presented in Appendix E. To investigate the impact of hardware improvements and to study the comparative performance at convergence, we vary the hardware parameters until convergence is achieved for the  $\text{CO}_2$  computations. With the 2-qubit gate fidelity improving one order of magnitude, we assume the one-qubit gate fidelities to also improve one order of magnitude. In the following, we represent hardware parameters in the format (prob. for 1-qubit error, prob. for 2-qubit error).

### A. Computation of ground state energies

In Fig. 2a, we present a histogram of the sampled VQE computations with current hardware parameters. While both algorithms exhibit large errors compared to the reference energy, the CEA demonstrates a significant improvement of accuracy, reducing the gap to quantum advantage substantially. With fewer qubits and shallower circuit depths, the CEA exhibits smaller sensitivity to noise as compared to the DM since the probabilities of qubit and gate errors are significantly reduced, leading to improved accuracy. It is essential to note that the increased accuracy of the CEA is obtained with less quantum resources as compared to the DM. Using current hardware parameters estimated to be  $(1.0 \times 10^{-3}, 1.0 \times 10^{-2})$  as reference points, we varied the hardware parameters until convergence was achieved, as depicted in Fig. 2d. Specifically, we achieve convergence at hardware parameters  $(0.5 \times 10^{-5}, 0.5 \times 10^{-4})$ . Note that the measured energy functional in the VQE algorithm,  $E[\theta]$ , is optimized according to the variational principle, yielding a guaranteed upper bound to the exact ground state energy. Therefore, the relevant subset of measurements are those which are minimal. For hardware parameters at convergence, a distribution of measure-

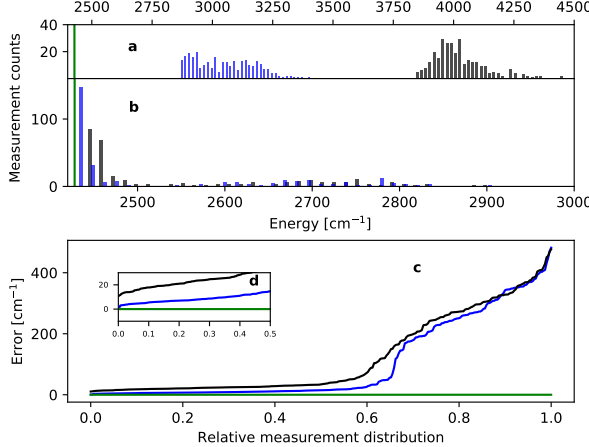


FIG. 2. Ground state energy calculations for the CEA and the DM with 300 VQE samples for each algorithm. Blue lines represent CEA measurements, black lines represent DM measurements and the green line represents the reference energy. Bin sizes of measurement samples are 35. Note the different axis scalings. **a)** Histogram of sampled VQE measurements with hardware parameters  $(1.0 \times 10^{-3}, 1.0 \times 10^{-2})$ . With current hardware parameters, the CEA provides a large increase of accuracy with an improvement of nearly  $1000 \text{ cm}^{-1}$ , reducing the quantum advantage gap substantially. **b)** Histogram of sampled VQE measurements with hardware parameters  $(0.5 \times 10^{-5}, 0.5 \times 10^{-4})$  at convergence. The subset of minimal energy measurements increases significantly for both algorithms with improving hardware parameters, which is advantageous in terms of the variational principle. The CEA, however, exhibits higher accuracy while being more resource-efficient. **c)** Cumulative distribution of VQE measurement errors with hardware parameters  $(0.5 \times 10^{-5}, 0.5 \times 10^{-4})$ . The error is calculated relative to the reference energy. **d)** Zoom of **c** with the convergence of CEA highlighted. Note the large subset of measurements which exhibit minimal error compared to the reference energy.

ment counts and a corresponding cumulative error distribution are presented in Figs. 2b and 2c. Results for both algorithms appear to accumulate at minimal energies. For both the CEA and the DM, there is a clear tendency to produce large subsets of minimal energy measurements which is both evident in the histogram and cumulative distribution of Figs. 2b and 2c. While both algorithms seem to produce relatively accurate results in Fig. 2d, with almost half of all measurements within an accuracy of  $< 20 \text{ cm}^{-1}$ , the CEA consistently achieves a higher accuracy and, at the same time, requires fewer quantum resources.

### B. Computation of excited state energies

The results of the QEOM computations for the excited state energies are presented for the CEA and the DM in Figs. 3 and 4 for which identical comparative conclusions as above may be made.

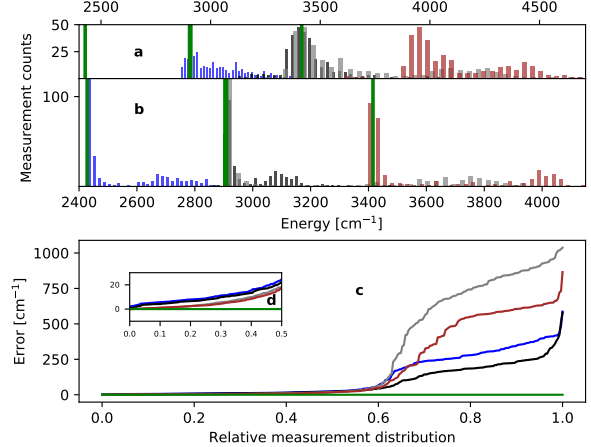


FIG. 3. Excited state energies for the CEA with 300 VQE samples. The lines represent the excited states as (blue, ground state), (black, first excited state), (gray, second excited state), (brown, third excited state) and the green lines represent the reference energies. The first and second excited states are degenerate. Bin sizes of measurement samples are 35. Note the different axis scalings. **a)** Histogram of sampled VQE measurements with hardware parameters  $(1.0 \times 10^{-3}, 1.0 \times 10^{-2})$ . **b)** Histogram of sampled VQE measurements with hardware parameters  $(0.5 \times 10^{-5}, 0.5 \times 10^{-4})$ . With improving hardware parameters, the excited state energies calculations converge to the reference energies using the QEOM algorithm analogously to the ground state calculations. **c)** Cumulative distribution of VQE measurement errors with hardware parameters  $(0.5 \times 10^{-5}, 0.5 \times 10^{-4})$ . The errors are calculated relative to the reference energies. **d)** Zoom of **c** with the convergence of CEA highlighted. Note the large subset of measurements which exhibit minimal error compared to the reference energies.

## V. CONCLUSION

In the short-term perspective, with a major increase of precision while utilizing fewer quantum resources, the route to quantum advantage for bosonic quantum simulations is substantially shorter for current hardware using the CEA. Furthermore, the reduction of quantum resources automatically allows for the study of larger molecular systems with current hardware. Most importantly, in the long-term perspective, the CEA may enable for the study of molecular systems with relevance in chemical, biological and medical applications. Finally, the algorithm allows for a flexible method to tailor the required quantum resources depending on the hardware parameters of the quantum computer. With the advantages being independent of hardware parameters along with the flexibility between qubit resources and quantum gate resources, our algorithm remains superior not only for current devices, but also for future fault-tolerant quantum devices.

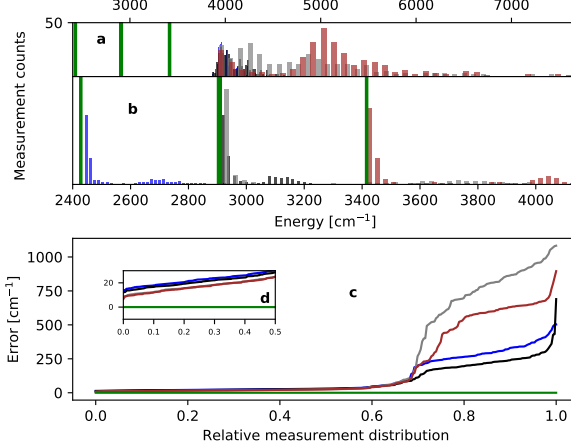


FIG. 4. Excited state energies for the DM with 300 VQE samples. The lines represent the excited states as (blue, ground state), (black, first excited state), (gray, second excited state), (brown, third excited state) and the green lines represent the reference energies. The first and second excited states are degenerate. Bin sizes of measurement samples are 35. Note the different axis scalings. **a)** Histogram of sampled VQE measurements with hardware parameters ( $1.0 \times 10^{-3}, 1.0 \times 10^{-2}$ ). **b)** Histogram of sampled VQE measurements with hardware parameters ( $0.5 \times 10^{-5}, 0.5 \times 10^{-4}$ ). With improving hardware parameters, the excited state energies calculations approach the reference energies, although without convergence as was observed using the CEA. **c)** Cumulative distribution of VQE measurement errors with hardware parameters ( $0.5 \times 10^{-5}, 0.5 \times 10^{-4}$ ). The errors are calculated relative to the reference energies. **d)** Zoom of **c**.

#### Appendix A: Bosonic many-body Hamiltonian in the $n$ -body expansion formalism

A many-body system of interacting bosons, in general, exhibit rather complicated interactions compared to, for example, electronic interactions in molecules. With electrons interacting through the two-body Coulomb interaction, bosons may interact through many-body coupling terms which further complicates the structure of the Hamiltonian. One way to parametrize a many-body system of interacting bosons is to expand the interaction term in a so-called  $n$ -body expansion. With the  $n$ -body expansion, one may obtain an accurate description of the anharmonicity of the potential, thus avoiding the intricate structure of Taylor expansions. The degrees of freedom of the bosonic system may be parametrized by a set of normal modes of vibrations,  $L$ . Each mode may be parametrized by a normal coordinate,  $q_l$ . The Hamiltonian reads

$$H = \sum_{l=0}^{L-1} \left( -\frac{1}{2} \frac{\partial^2}{\partial q_l^2} \right) + V(\{q_l\}). \quad (\text{A1})$$

Following Christiansen [22] and Ollitrault [15], the potential in the  $n$ -body expansion may be written as

$$V(\{q_l\}) = V_0 + \sum_{l=0}^{L-1} V^{[l]}(q_l) + \sum_{l < m} V^{[lm]}(q_l, q_m) + \dots \quad (\text{A2})$$

In this expansion, the first term contains the equilibrium configuration energy and the latter sums represent higher-order mode couplings. For the first sum,  $q_l$  is varied and all other coordinates remain in their equilibrium configuration. For the second sum,  $q_l$  and  $q_m$  are varied with all other coordinates in equilibrium, i.e. introducing two-body couplings. The expansion of Eq. A2 may be truncated to a given order  $n$ . One may note that the Hamiltonian exhibits a variety of symmetries. These symmetries include conservation of modal excitations in the sense that all vibrational modes contain only one excitation of a modal at any time. Furthermore, such a modal is confined to its mode. This gives rise to a mode-conserving excitation manifold.

The spectrum of a given mode  $l$  may be divided into a subspace of  $N_l$  modals. The modal basis set for mode  $l$  is given by a set of functions [21]

$$S_l = \{\phi_0^{(l)}(q_l), \dots, \phi_{N_l-1}^{(l)}(q_l)\}. \quad (\text{A3})$$

The total wavefunction of the system will be a linear combination of all possible product wavefunctions of modals from each mode, called Hartree products,

$$|\psi\rangle = \sum_{k_0}^{N_0} \dots \sum_{k_{L-1}}^{N_{L-1}} C_{k_0 \dots k_{L-1}} \phi_{k_0}^{(0)}(q_1) \dots \phi_{k_{L-1}}^{(L)}(q_{L-1}). \quad (\text{A4})$$

In the second quantization formalism, a Hartree product is given by

$$|\Phi_{\mathbf{r}}\rangle = \prod_{l=0}^{L-1} a_{r^l}^{l\dagger} |0\rangle \quad (\text{A5})$$

where  $\mathbf{r} = [r^0, \dots, r^{L-1}]^T$  is a vector designating the indices of the occupied modals in the product. Thus, a given modal occupation may be represented by an integer in the interval  $r^l \in \{0, \dots, N_l - 1\}$ . Conventionally, the modal functions are mean field solutions to the Hamiltonian and may be solved using, for example, vibrational self consistent field (VSCF) methods [22].

#### Appendix B: Dimensional scaling of the Hamming truncation

The Hamming truncation provides a flexible method to utilize quantum resources efficiently depending on the hardware parameters of the quantum computer. Depending on whether qubit or quantum gate resources are the limiting factor of the experimental implementation of the quantum computer, one may perform the Hamming truncation such that it satisfies the preferences of the hardware parameters.

Consider a qubit register of size  $N$ . For such a register, there

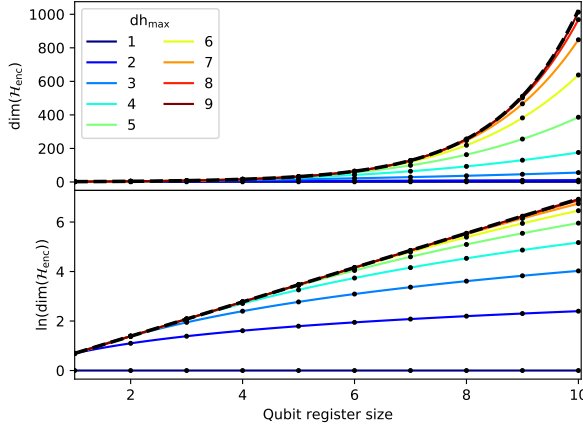


FIG. 5. Dimension of the subspace of the qubit Hilbert space available for encoding,  $\mathcal{H}_{\text{enc}}$ , as a function of the qubit register size for  $\Lambda_{\text{CEA}}$ . The dimensional scaling of the encoding subspace is presented for a variety of Hamming truncations,  $\text{dh}_{\text{max}}$ . With decreasing Hamming truncation (increasing  $\text{dh}_{\text{max}}$ ), more qubit states are available for encoding and thus the dimensional scaling approaches the non-truncated exponential scaling. For all Hamming truncations, the qubit memory advantage for  $\Lambda_{\text{CEA}}$  compared to  $\Lambda_{\text{DM}}$  is polynomial and scales as  $\dim(\mathcal{H}_{\text{enc}}^{\text{CEA}}) \sim \mathcal{O}(N^{\text{dh}_{\text{max}}})$  with  $N$  being the qubit register size and  $\text{dh}_{\text{max}}$  being the Hamming truncation.

would be  $N - 1$  available Hamming truncations. With no truncation, the compact encoding provides an exponential increase in  $\dim(\mathcal{H}_{\text{enc}})$  as function of qubit register size. For the DM, the dimensional scaling of the encoding subspace is linear with

$$\dim(\mathcal{H}_{\text{enc}}^{\text{DM}}) \sim \mathcal{O}(N). \quad (\text{B1})$$

For all  $N - 1$  truncations for the CEA, the qubit memory advantage scales polynomially with

$$\dim(\mathcal{H}_{\text{enc}}^{\text{CEA}}) \sim \mathcal{O}(N^{\text{dh}_{\text{max}}}) \quad (\text{B2})$$

with  $\text{dh}_{\text{max}}$  being the Hamming truncation. Thus, for any Hamming truncation, the CEA provides a polynomial advantage in qubit memory as compared to the DM. The dimensional scalings of the available encoding subspace as a function of qubit register size is depicted in Fig. 5. As is expected, with decreasing Hamming truncation, the polynomial scaling approaches the exponential scaling of the encoding subspace. With quantum devices typically favoring either qubit or quantum gate resources, one may utilize the resources of the quantum device efficiently by appropriately performing the Hamming truncation.

### Appendix C: Unitary coupled cluster theory

The UCC ansatz reads

$$|\text{UCC}\rangle = e^{T - T^\dagger} |\Phi_s\rangle \quad (\text{C1})$$

where  $T$  is the cluster operator and  $|\Phi_s\rangle$  is a reference Hartree product with a reference modal configuration given by  $\mathbf{s}$ . Typically, only single and double excitations of the above ansatz are sufficient for accurate calculations. The single and double cluster operators read

$$T_1 = \sum_{l=0}^{L-1} \sum_{r^l} t_{r^l}^l a_{r^l}^{l\dagger} a_{s^l}^l \quad (\text{C2})$$

and

$$T_2 = \sum_{l < m} \sum_{r^l} \sum_{p^m} t_{r^l p^m}^{lm} a_{r^l}^{l\dagger} a_{p^m}^{m\dagger} a_{s^l}^l a_{q^m}^m \quad (\text{C3})$$

with  $r^l, p^m$  and  $s^l, q^m$  being unoccupied and occupied modals, respectively, and  $t_{r^l}^l, t_{r^l p^m}^{lm} \in \mathbb{R}$ . Thus, the UCC ansatz generates a linear combination of single (double) excitations out of the reference Hartree product while confining each modal excitation within the same mode.

### Appendix D: Comparison of quantum gate resource requirements

When implementing the Trotter decomposed UCC cluster operator on a quantum computer, the exponentiated Pauli operators are typically realized using the ladder method of concatenated CNOT gates [13]. In terms of CNOT gate resource requirements, both the DM and the CEA scale quadratically with the number of modal states but with different coefficients. This is demonstrated in the following. The amount of CNOT gates required to implement an exponentiated product of  $p$  Pauli operators in a quantum computer is given by  $n_{\text{CNOT}} = 2(p - 1)$ . Assuming  $N_l = N$  for all modes, the amount of qubit states with  $\text{dh} = i$  are denoted  $N_i$  such that  $\sum_i N_i = N - 1$ . Analytical estimations for the number of CNOT gates required to implement the UCC ansatz in a quantum computer are presented in Table I for  $\text{dh}_{\text{max}} = 3$  with  $n$  being the mode-coupling truncation of the Hamiltonian.

Mapping	Cluster operator	CNOTs
DM	$T_1$	$4L(N - 1)$
DM	$T_2$	$48 \binom{L}{n} (N - 1)^2$
CEA	$T_1$	$4LN_2$
CEA	$T_2$	$\binom{L}{n} (4N_1^2 + 48N_2^2 + 32N_1N_2)$

TABLE I. Analytical estimations of the number of CNOT gates required to implement the UCC ansatz using the DM and the CEA.

Considering the expressions for the DM in Table I, all qubit states require an equal amount of CNOT gates since the Hamming distance is constant for all states. For the CEA, the reduction of resources is evident. For  $T_1$ , only states with  $\text{dh} = 2$  require CNOT gates for implementation. For  $T_2$ , states with  $\text{dh} = 1$  and combinations of  $\text{dh} = 1$  and  $\text{dh} = 2$  require less resources as compared to the DM.

## Appendix E: Numerical simulation details

All VQE simulations were performed using the IBM Qiskit software package [25]. Since the CEA is not implemented in Qiskit, an extended version of Qiskit was developed and may be obtained on request to the authors. To simulate a noisy device, we used the Qiskit QASM simulator. With four vibrational modes and two modal wavefunctions per mode, we allocated four qubit registers of size one (4 qubits) for the CEA and four qubit registers of size two (8 qubits) for the DM. For the optimization in the VQE, we used the COBYLA optimization routine. The ground state optimization of CO<sub>2</sub> was performed using density functional theory (B3LYP) with the 6-31g basis set in Gaussian16 [26] using the Qiskit interface. The electronic potential energy surface (PES) was constructed using the GaussianForcesDriver in Qiskit [15]. This involves the approximation of the PES as a quartic force field

with semi-numerical differentiation of the analytical Hessian. In the computation of the matrix elements of the  $n$ -body expansion Hamiltonian of Eq. A1, a harmonic oscillator basis set was used. Since the subject of this work is to study the relative performance of the CEA and the DM, the particular choice of basis set is not important and the results found here apply for other basis sets as well.

## ACKNOWLEDGMENTS

We are grateful to Ove Christiansen, Pauline Ollitrault and Ivano Tavernelli for helpful and insightful discussions in relation to this work. The numerical results presented in this work were obtained at the Centre for Scientific Computing, Aarhus, <http://phys.au.dk/forskning/cscaa/>. The authors acknowledge support from the Independent Research Fund Denmark, the Carlsberg Foundation, and the Aarhus University Research Foundation.

---

[1] S. Lloyd, “Universal quantum simulators,” *Science*, vol. 273, no. 5278, pp. 1073–1078, 1996.

[2] J. Preskill, “Quantum Computing in the NISQ era and beyond,” *Quantum*, vol. 2, p. 79, Aug. 2018.

[3] P. K. Barkoutsos, J. F. Gonthier, I. Sokolov, N. Moll, G. Salis, A. Fuhrer, M. Ganzhorn, D. J. Egger, M. Troyer, A. Mezzacapo, S. Filipp, and I. Tavernelli, “Quantum algorithms for electronic structure calculations: Particle-hole Hamiltonian and optimized wave-function expansions,” *Physical Review A*, vol. 98, p. 022322, Aug. 2018.

[4] A. Peruzzo, J. McClean, P. Shadbolt, M.-H. Yung, X.-Q. Zhou, P. J. Love, A. Aspuru-Guzik, and J. L. O’Brien, “A variational eigenvalue solver on a photonic quantum processor,” *Nature Communications*, vol. 5, Jul 2014.

[5] A. Kandala, A. Mezzacapo, K. Temme, M. Takita, M. Brink, J. M. Chow, and J. M. Gambetta, “Hardware-efficient variational quantum eigensolver for small molecules and quantum magnets,” *Nature (London)*, vol. 549, pp. 242–246, Sept. 2017.

[6] N. P. D. Sawaya, T. Menke, T. H. Kyaw, S. Johri, A. Aspuru-Guzik, and G. G. Guerreschi, “Resource-efficient digital quantum simulation of d-level systems for photonic, vibrational, and spin-s hamiltonians,” *npj Quantum Information*, vol. 6, Jun 2020.

[7] O. Di Matteo, A. McCoy, P. Gysbers, T. Miyagi, R. M. Woloshyn, and P. Navrátil, “Improving Hamiltonian encodings with the Gray code,” *arXiv e-prints*, p. arXiv:2008.05012, Aug. 2020.

[8] F. Arute, K. Arya, R. Babbush, D. Bacon, J. C. Bardin, R. Barends, S. Boixo, M. Broughton, B. B. Buckley, D. A. Buell, B. Burkett, N. Bushnell, Y. Chen, Z. Chen, B. Chiaro, R. Collins, W. Courtney, S. Demura, A. Dunsworth, D. Eppens, E. Farhi, A. Fowler, B. Foxen, C. Gidney, M. Giustina, R. Graff, S. Habegger, M. P. Harrigan, A. Ho, S. Hong, T. Huang, W. J. Huggins, L. Ioffe, S. V. Isakov, E. Jeffrey, Z. Jiang, C. Jones, D. Kafri, K. Kechedzhi, J. Kelly, S. Kim, P. V. Klimov, A. Korotkov, F. Kostritsa, D. Landhuis, P. Laptev, M. Lindmark, E. Lucero, O. Martin, J. M. Martinis, J. R. McClean, M. McEwen, A. Megrant, X. Mi, M. Mohseni, W. Mruczkiewicz, J. Mutus, O. Naaman, M. Neeley, C. Neill, H. Neven, M. Yuezen Niu, T. E. O’Brien, E. Ostby, A. Petukhov, H. Putterman, C. Quintana, P. Roushan, N. C. Rubin, D. Sank, K. J. Satzinger, V. Smelyanskiy, D. Strain, K. J. Sung, M. Szalay, T. Y. Takeshita, A. Vainsencher, T. White, N. Wiebe, Z. J. Yao, P. Yeh, and A. Zalcman, “Hartree-Fock on a superconducting qubit quantum computer,” *Science*, vol. 369, pp. 1084–1089, Aug. 2020.

[9] J. I. Colless, V. V. Ramasesh, D. Ahlen, M. S. Blok, M. E. Kimchi-Schwartz, J. R. McClean, J. Carter, W. A. de Jong, and I. Siddiqi, “Computation of molecular spectra on a quantum processor with an error-resilient algorithm,” *Phys. Rev. X*, vol. 8, p. 011021, Feb 2018.

[10] N. P. D. Sawaya, F. Paesani, and D. P. Tabor, “Near- and long-term quantum algorithmic approaches for vibrational spectroscopy,” 2020.

[11] A. Aspuru-Guzik, A. D. Dutoi, P. J. Love, and M. Head-Gordon, “Simulated quantum computation of molecular energies,” *Science*, vol. 309, no. 5741, pp. 1704–1707, 2005.

[12] J. Romero, R. Babbush, J. R. McClean, C. Hempel, P. J. Love, and A. Aspuru-Guzik, “Strategies for quantum computing molecular energies using the unitary coupled cluster ansatz,” *Quantum Science and Technology*, vol. 4, p. 014008, oct 2018.

[13] S. McArdle, S. Endo, A. Aspuru-Guzik, S. C. Benjamin, and X. Yuan, “Quantum computational chemistry,” *Rev. Mod. Phys.*, vol. 92, p. 015003, Mar 2020.

[14] S. McArdle, A. Mayorov, X. Shan, S. Benjamin, and X. Yuan, “Digital quantum simulation of molecular vibrations,” *Chem. Sci.*, vol. 10, pp. 5725–5735, 2019.

[15] P. J. Ollitrault, A. Baiardi, M. Reiher, and I. Tavernelli, “Hardware efficient quantum algorithms for vibrational structure calculations,” *Chem. Sci.*, vol. 11, pp. 6842–6855, 2020.

[16] D. A. Fedorov, M. J. Otten, S. K. Gray, and Y. Alexeev, “Ab Initio Molecular Dynamics on Quantum Computers,” *arXiv e-prints*, p. arXiv:2008.06562, Aug. 2020.

[17] F. F. Crim, “Chemical dynamics of vibrationally excited molecules: Controlling reactions in gases and on surfaces,”

*Proceedings of the National Academy of Sciences*, vol. 105, no. 35, pp. 12654–12661, 2008.

[18] H. Hwang and P. J. Rossky, “Harmonic model description of the franck-condon density for a betaine dye molecule,” *The Journal of Physical Chemistry A*, vol. 108, no. 14, pp. 2607–2616, 2004.

[19] C. Zhu, K. K. Liang, M. Hayashi, and S. H. Lin, “Theoretical treatment of anharmonic effect on molecular absorption, fluorescence spectra, and electron transfer,” *Chemical Physics*, vol. 358, no. 1, pp. 137 – 146, 2009.

[20] T. wei Huang, L. Yang, C. Zhu, and S. H. Lin, “Absorption and fluorescence spectra of the neutral and anionic green fluorescent protein chromophore: Franck-condon simulation,” *Chemical Physics Letters*, vol. 541, pp. 110 – 116, 2012.

[21] O. Christiansen, “A second quantization formulation of multi-mode dynamics,” *The Journal of Chemical Physics*, vol. 120, no. 5, pp. 2140–2148, 2004.

[22] O. Christiansen, “Vibrational coupled cluster theory,” *The Journal of Chemical Physics*, vol. 120, no. 5, pp. 2149–2159, 2004.

[23] M. A. Nielsen and I. L. Chuang, *Quantum Computation and Quantum Information: 10th Anniversary Edition*. USA: Cambridge University Press, 10th ed., 2011.

[24] P. J. Ollitrault, A. Kandala, C.-F. Chen, P. K. Barkoutsos, A. Mezzacapo, M. Pistoia, S. Sheldon, S. Woerner, J. M. Gambetta, and I. Tavernelli, “Quantum equation of motion for computing molecular excitation energies on a noisy quantum processor,” *Phys. Rev. Research*, vol. 2, p. 043140, Oct 2020.

[25] H. Abraham, AduOffei, R. Agarwal, I. Y. Akhalwaya, G. Aleksandrowicz, T. Alexander, M. Amy, E. Arbel, Arijit02, A. Asfaw, A. Avkhadiev, C. Azaustre, AzizNgoueya, A. Banerjee, A. Bansal, P. Barkoutsos, A. Barnawal, G. Barron, G. S. Barron, L. Bello, Y. Ben-Haim, D. Bevenius, A. Bhobe, L. S. Bishop, C. Blank, S. Bolos, S. Bosch, Brandon, S. Bravyi, Bryce-Fuller, D. Bucher, A. Burov, F. Cabrera, P. Calpin, L. Capelluto, J. Carballo, G. Carrascal, A. Chen, C.-F. Chen, E. Chen, J. C. Chen, R. Chen, J. M. Chow, S. Churchill, C. Claus, C. Clauss, R. Cocking, F. Correa, A. J. Cross, A. W. Cross, S. Cross, J. Cruz-Benito, C. Culver, A. D. Córcoles-Gonzales, S. Dague, T. E. Dandachi, M. Daniels, M. Dartialh, Davide-Frr, A. R. Davila, A. Dekusar, D. Ding, J. Doi, E. Drechsler, Drew, E. Dumitrescu, K. Dumon, I. Duran, K. EL-Safty, E. Eastman, G. Eberle, P. Eendebak, D. Egger, M. Everitt, P. M. Fernández, A. H. Ferrera, R. Foulland, FranckChevallier, A. Frisch, A. Fuhrer, B. Fuller, M. GEORGE, J. Gacon, B. G. Gago, C. Gambella, J. M. Gambetta, A. Gammanpila, L. Garcia, T. Garg, S. Garion, A. Gilliam, A. Giridharan, J. Gomez-Mosquera, Gonzalo, S. de la Puente González, J. Gorzinski, I. Gould, D. Greenberg, D. Grinko, W. Guan, J. A. Gunnels, M. Haglund, I. Haide, I. Hamamura, O. C. Hamido, F. Harkins, V. Havlicek, J. Hellmers, Ł. Herok, S. Hillmich, H. Horii, C. Howington, S. Hu, W. Hu, J. Huang, R. Huisman, H. Imai, T. Imamichi, K. Ishizaki, R. Iten, T. Itoko, JamesSeaward, A. Javadi, A. Javadi-Abhari, W. Javed, Jessica, M. Jivrajani, K. Johns, S. Johnstun, Jonathan-Shoemaker, V. K., T. Kachmann, A. Kale, N. Kanazawa, Kang-Bae, A. Karazeev, P. Kassebaum, J. Kelso, S. King, Knabberjoe, Y. Kobayashi, A. Kovyrshin, R. Krishnakumar, V. Krishnan, K. Krsulich, P. Kumkar, G. Kus, R. LaRose, E. Lacal, R. Lambert, J. Lapeyre, J. Latone, S. Lawrence, C. Lee, G. Li, D. Liu, P. Liu, Y. Maeng, K. Majmudar, A. Malyshev, J. Manela, J. Marecek, M. Marques, D. Maslov, D. Mathews, A. Matsuo, D. T. McClure, C. McGarry, D. McKay, D. McPherson, S. Meesala, T. Metcalfe, M. Mevissen, A. Meyer, A. Mezzacapo, R. Midha, Z. Minev, A. Mitchell, N. Moll, J. Montanez, G. Monteiro, M. D. Mooring, R. Morales, N. Moran, M. Motta, MrF, P. Murali, J. Müggenburg, D. Nadlinger, K. Nakanishi, G. Nannicini, P. Nation, E. Navarro, Y. Naveh, S. W. Neagle, P. Neuweiler, J. Nicander, P. Niroula, H. Norlen, NuoWen-Lei, L. J. O’Riordan, O. Ogunbayo, P. Ollitrault, R. Otaolea, S. Oud, D. Padilha, H. Paik, S. Pal, Y. Pang, V. R. Pasczuzzi, S. Perriello, A. Phan, F. Piro, M. Pistoia, C. Piveteau, P. Pocreau, A. Pozas-iKerstjens, M. Prokop, V. Prutyanov, D. Puzzuoli, J. Pérez, Quintiii, R. I. Rahman, A. Raja, N. Ramagiri, A. Rao, R. Raymond, R. M.-C. Redondo, M. Reuter, J. Rice, M. Riedemann, M. L. Rocca, D. M. Rodríguez, RohithKarur, M. Rossmannek, M. Ryu, T. SAPV, SamFer-racin, M. Sandberg, H. Sandesara, R. Sapra, H. Sargsyan, A. Sarkar, N. Sathaye, B. Schmitt, C. Schnabel, Z. Schoenfeld, T. L. Scholten, E. Schouste, J. Schwarm, I. F. Sertage, K. Setia, N. Shammah, Y. Shi, A. Silva, A. Simonetto, N. Sing-stock, Y. Siraichi, I. Sitzdikov, S. Sivarajah, M. B. Sletfjerd-ing, J. A. Smolin, M. Soeken, I. O. Sokolov, I. Sokolov, SooluThomas, Starfish, D. Steenken, M. Stypulkoski, S. Sun, K. J. Sung, H. Takahashi, T. Takawale, I. Tavernelli, C. Tay-lor, P. Taylor, S. Thomas, M. Tillet, M. Tod, M. Tomasik, E. de la Torre, K. Trabing, M. Treinish, TrishaPe, D. Tulsi, W. Turner, Y. Vaknin, C. R. Valcearce, F. Varchon, A. C. Vazquez, V. Villar, D. Vogt-Lee, C. Vuillot, J. Weaver, J. Weidenfeller, R. Wieczorek, J. A. Wildstrom, E. Winston, J. J. Woehr, S. Woerner, R. Woo, C. J. Wood, R. Wood, S. Wood, S. Wood, J. Wootton, D. Yeralin, D. Yonge-Mallo, R. Young, J. Yu, C. Zachow, L. Zdanski, H. Zhang, C. Zoufal, Zoufalc, a kapila, a matsuo, bcamorrison, brandhsn, nick bronn, brosand, chlorophyll zz, csseifms, dekel.meirom, dekelmeirom, dekoool, dime10, drholmie, dtrenev, ehchen, elfrocampedor, faisalde-bouni, fanizzamarco, gabrieleagl, gadijal, galeinston, georgios ts, gruu, hhori, hykavitha, jagunther, jliu45, jscott2, kane-jess, klinvill, krutik2966, kurarr, lerongil, ma5x, merav aharoni, michelle4654, ordmoj, sagar pahwa, rmoyer, saswati qiskit, scottkelso, sethmerkel, shaashwat, sternparky, strickro-man, sumitpuri, tigerjack, toural, tsura crisaldo, vvilpas, welien, willhang, yang.luh, yotamvakninibm, and M. Čepulkovskis, “Qiskit: An open-source framework for quantum computing,” 2019.

[26] M. J. Frisch, G. W. Trucks, H. B. Schlegel, G. E. Scuse-ria, M. A. Robb, J. R. Cheeseman, G. Scalmanni, V. Barone, G. A. Petersson, H. Nakatsuji, X. Li, M. Caricato, A. V. Marenich, J. Bloino, B. G. Janesko, R. Gomperts, B. Mennucci, H. P. Hratchian, J. V. Ortiz, A. F. Izmaylov, J. L. Sonnenberg, D. Williams-Young, F. Ding, F. Lippurini, F. Egidi, J. Goings, B. Peng, A. Petrone, T. Henderson, D. Ranasinghe, V. G. Zakrajewski, J. Gao, N. Rega, G. Zheng, W. Liang, M. Hada, M. Ehara, K. Toyota, R. Fukuda, J. Hasegawa, M. Ishida, T. Nakajima, Y. Honda, O. Kitao, H. Nakai, T. Vreven, K. Throssell, J. A. Montgomery, Jr., J. E. Peralta, F. Ogliaro, M. J. Bearpark, J. J. Heyd, E. N. Brothers, K. N. Kudin, V. N. Staroverov, T. A. Keith, R. Kobayashi, J. Normand, K. Raghavachari, A. P. Rendell, J. C. Burant, S. S. Iyengar, J. Tomasi, M. Cossi, J. M. Millam, M. Klene, C. Adamo, R. Cammi, J. W. Ochterski, R. L. Martin, K. Morokuma, O. Farkas, J. B. Foresman, and D. J. Fox, “Gaussian™16 Re-  
vision C.01,” 2016. Gaussian Inc. Wallingford CT.